


## Strain-induced topological phase transition in graphene nanoribbons

Anhua Huang <sup>1,2</sup>, Shasha Ke <sup>1,2</sup>, Ji-Huan Guan <sup>1,2</sup>, Jun Li <sup>3</sup>, and Wen-Kai Lou <sup>1,2,\*</sup>

<sup>1</sup>SKLSM, Institute of Semiconductors, Chinese Academy of Sciences, Beijing 100083, China

<sup>2</sup>College of Materials Science and Opto-electronic Technology, Center of Materials Science and Optoelectronics Engineering, University of Chinese Academy of Sciences, Beijing 100049, China

<sup>3</sup>Department of Physics, School of Physical Science and Technology, Xiamen University, Xiamen 361005, China

 (Received 3 July 2023; revised 19 September 2023; accepted 12 December 2023; published 10 January 2024)

The electronic properties of two-dimensional (2D) nanostructures are highly responsive to changes in their geometry, making strain-engineering a powerful method for tuning the electronic characteristics of flexible 2D nanostructures. Quasi-one-dimensional (1D) graphene nanoribbons (GNRs) are crucial quantum building blocks in the development of next-generation flexible devices and have recently been recognized for possessing distinct symmetry-protected topological phases characterized by a  $Z_2$  invariant. In this study, utilizing the tight-binding (TB) model, we present compelling evidence that the topological phase transition in 1D GNRs can be effectively controlled through strain-engineering. Furthermore, we investigate the behavior of heterojunctions composed of different types of AGNR segments and reveal that strain can create or eliminate the junction state while significantly enhancing the end states. Our study presents a new method for tuning topological phase transitions in flexible quasi-1D materials, offering an efficient way to control over junction state and end states.

DOI: [10.1103/PhysRevB.109.045408](https://doi.org/10.1103/PhysRevB.109.045408)

### I. INTRODUCTION

Topological phases of matter, having a gapped spectrum in bulk and supporting a metallic edge excitation robust against symmetry-respecting perturbation, have attracted tremendous interest in the past decades. In contrast to the general wisdom of Landau-Ginzburg field theory, the topological phases share the same symmetry as a trivial insulator and still are different phases, which are characterized by topological invariants [1–10]. Since the discovery of topological quantum materials [1–10], studies on the topology have mostly focused on two-dimensional (2D) [3–5,7–10] and three-dimensional (3D) [6,11] systems for many years. Recently, there is a rapidly growing interest to study the topology of one-dimensional (1D) systems such as graphene nanoribbons (GNRs) which have additional rich physics and are different from other dimensions [12–22].

With the advancement of precision chemistry, it has become feasible to synthesize GNRs through bottom-up approaches using precursor molecules. These techniques enable the atomically precise design of a wide range of GNRs, allowing for control over their edge shapes, widths, terminations, and dopant atoms [23–27]. GNRs, as one-dimensional (1D) systems, exhibit tunable electronic structures that hold great promise for applications in material science, nanodevices, and transport devices [28–32]. The topology classification of various GNRs, characterized by the  $Z_2$  invariant and  $Z$  index, has been extensively studied [12,14,22]. For instance, the  $Z_2$  invariant has been determined for armchair graphene nanoribbons (AGNRs) [12], cove-edged GNRs, chevron GNRs [14],

cove-edged zigzag graphene nanoribbons (ZGNR-Cs) [22], and chiral graphene nanoribbons [33]. These  $Z_2$  invariants are influenced by factors such as the ribbon width, symmetry, and geometric boundaries of the unit cell. Intriguingly, theoretical predictions [12,14] and experimental verifications [16] have demonstrated the existence of topological junction state in 1D superlattices formed by alternating segments of GNRs with distinct topological properties.

The ability to effectively and controllably adjust the topological invariants of materials is a crucial area of research, with implications both in fundamental physics and practical applications of topological insulators. In 2D and 3D systems, extensive studies have investigated the transition between the topological trivial phase and the topological nontrivial phase using various methods including the application of external electric fields [34], temperature variations [35], alloying [36,37], asymmetry [38], polarization effects [39], and interface engineering [40]. Through density-functional theory (DFT) and tight-binding (TB) calculations, Refs. [41] and [42] conducted an in-depth and comprehensive study on the gap engineering through the strain of graphene nanoribbon and found the band gap  $E_g$  of AGNRs can be closed and reopened. However, in the context of 1D systems, the method for tuning topological phases has only been proposed by Zhao *et al.*, who employed intricate and precise techniques involving the addition of boron-nitrogen atoms and external transverse electric fields [21].

In this study, we propose a novel approach to achieve topological phase transition in flexible 1D AGNRs through the application of external strain. The graphene monolayer has been experimentally demonstrated to possess high mechanical strength, allowing them to withstand elastic strains up to 25% and enabling the design of arbitrary strain patterns [43,44].

\*wklou@semi.ac.cn

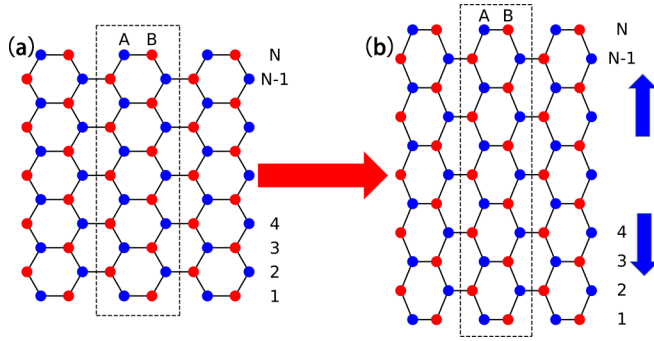


FIG. 1. Geometry of AGNR. The illustration of unstrained AGNR (a) and strained AGNR (b). The blue and red balls represent A and B sublattice, respectively. The black dashed rectangular region depicts a unit cell of the AGNR, which is commensurate with a zigzag end termination. The unit cell contains  $2N$  atoms, where  $N$  corresponds to AGNRs with different widths. The two blue arrows represent the direction of the strain.

Concurrently, the system undergoes a topological phase transition, leading to a change in the  $Z_2$  invariant from 1 to 0 or from 0 to 1, depending on the width of the AGNRs. And multiple topological phase transitions can occur with larger strain. This transition is characterized by the interchange of the parity eigenvalues of the wave function at the conduction-band minimum (CBM) and valence-band maximum (VBM). Furthermore, in heterojunctions composed of different types of AGNR segments, we observe the emergence of a junction state localized at the interface of the heterojunction, as well as the presence of end states localized at the ends of the ribbons, consistent with previous studies. Interestingly, the application of the strain can create or eliminate the junction state, while simultaneously enhancing the end states. Our study presents a new method for tuning topological phase transitions in flexible quasi-1D materials, offering an effective approach to control over junction state and end states.

This paper is organized as follows. Section II provides a detailed description of the strain form used in the study, along with the TB model employed for AGNRs. The discussion of the Zak phase is also included in this section. In Sec. III, we present the numerical results, which include an analysis of the band structure for AGNRs with varying widths, an examination of the influence of the strain on the  $E_g$ , and an investigation into the ability of the strain to induce topological phase transitions in AGNRs. Finally, in Sec. IV, we provide a concise summary of the findings presented in this paper.

## II. MODEL AND THEORY

The geometry of AGNR is shown in Fig. 1(a). A graphene ribbon consists of two sublattices, denoted as A and B, represented by blue and red colors, respectively. The width of AGNR, denoted as  $N$ , is determined by the number of A (B) atoms in a unit cell and the real width is given by  $W = Na_0/2$ , where  $a_0$  is the lattice constant of graphene. In this study, we focus on AGNRs with  $N$  being odd and commensurate with a zigzag end termination, which ensures the unit cells possess inversion or mirror symmetry [12]. In general, strain can significantly modify the electronic spectrum of a

honeycomb lattice, leading to intriguing physical phenomena such as valley filter [45], manipulation of edge states [46], valley-dependent Brewster angles, and Goos-Hänchen effect [47]. For AGNRs, previous studies have shown that strain with the form  $u_x = cy^2$  induces a pseudogauge field  $A(r)$  in the Dirac equation, resulting in quasiflat Landau levels [48,49]. In this study, we consider the strain form  $u_y = f(y)$ . Here,  $f(y)$  is an arbitrary function about  $y$ . Importantly, the strain-induced topological phase transition does not rely on the specific form of the strain  $f(y)$ . In fact, any function  $f(y)$  about  $y$  can be expanded by Taylor series. We have calculated different strain forms, including strain forms of linear terms, quadratic terms, and cubic terms, and found that all of them effectively control the topological phase transition in AGNRs, yielding consistent conclusions. For simplicity, we consider the homogeneous strain with

$$u_y = cy \quad (1)$$

shown by blue arrows in Fig. 1(b), as a typical example to demonstrate topological phase transition driven by the strain effect in AGNRs. It is reported that nonlinear effects that arise for deformation strengths greater than about 20% of the lattice constant of graphene are significant [50,51]. For our case, the maximum change of the lattice constant is smaller than the 8%, which is two times smaller than the 20% for the original lattice constant. Therefore, we can safely neglect the nonlinear strain effects. Results for the other three strain forms are presented in the Supplemental Material [52].

The AGNRs can be well described by a TB model with one  $\pi$  electron per atom, which can be written as

$$H = \sum_i \epsilon_i a_i^\dagger a_i - \sum_{(ij)} t a_i^\dagger a_j + \text{H.c.}, \quad (2)$$

where  $a_i^\dagger$  and  $a_i$  are the creation and annihilation operators, respectively, for an electron on the lattice site  $i$  and onsite energy  $\epsilon_i$ . The second term  $t$  is the hopping parameter between site  $i$  and site  $j$ . When considering the strain described by Eq. (1), the hopping parameter  $t$  becomes position dependent instead of constant and should be replaced by the relation  $t = t_0 e^{-\beta(d/a_{cc}-1)}$  [53]. Here,  $t_0$  is the original unstrained hopping parameter,  $\beta$  is about the strength of the distance-dependent hopping modulation,  $d$  is the strained distance between two atoms, and  $a_{cc} = a_0/\sqrt{3}$  is the unstrained carbon-carbon distance. Using the Pybinding [54] and PythTB package [55], we can get the electronic properties of the system.

The Zak phase, which refers to Berry's phase [12,56] gathered up by a particle moving across the Brillouin zone (BZ), characterizes the symmetry-protected topological (SPT) phases in a 1D periodic system. It can be obtained by an integral of the Berry connection,  $i \langle \varphi_{nk} | \nabla_k \varphi_{nk} \rangle$  across the 1D BZ as follows:

$$\gamma_n = i(2\pi/L) \int_{-\pi/L}^{\pi/L} dk \langle \varphi_{nk} | \nabla_k \varphi_{nk} \rangle, \quad (3)$$

where  $L$  is the unit cell size,  $k$  is the wave vector, and  $\varphi_{nk}$  is the the periodic part of the electronic Bloch wave function in band  $n$ . The Zak phase could be written in two parts  $\gamma_n = \gamma_{1,n} + \gamma_{2,n}$  [15,57]. The former part of the Zak phase is an intracell quantity that depends on the specific spatial origin

and the choice of the unit cell. On the other hand, the latter part is an intercell quantity that is purely defined in  $k$  space and is based on the Bloch wave function. In general, the Zak phase is sensitive to the shape of the unit cell and can take on various values. However, if the system possesses spatial symmetries such as inversion  $\hat{I}$  and/or mirror  $\hat{M}$ , the Zak phase of a band becomes quantized at either 0 or  $\pi$ . A Zak phase of 0 corresponds to a topological trivial band, while a Zak phase of  $\pi$  indicates a topological nontrivial band [12,56].

In 1D AGNRs, the SPT phase of a band insulator is determined by the sum of the Zak phases of all the occupied bands. To characterize the topology of AGNRs, we use the  $Z_2$  invariant [7]. The  $Z_2$  invariant can be calculated by [12]

$$(-1)^{Z_2} = e^{i \sum_n \gamma_n}, \quad (4)$$

where the sum is over the occupied bands. The  $Z_2 = 1(0)$  indicates a topological nontrivial (trivial) insulator.

In addition to the TB model, we perform additional calculations using the Vienna *ab initio* simulation package (VASP) code [58,59] to further validate the influence of the strain on the electronic structure of AGNRs. In our DFT calculations, we employ the Perdew-Burke-Ernzerhof (PBE) exchange-correlation functional [60]. To ensure accuracy, a  $13 \times 1 \times 1$  Monkhorst-Pack  $k$  mesh is used to sample the BZ, and a substantial vacuum region exceeding  $20 \text{ \AA}$  is included in the  $y$  and  $z$  direction. The plane-wave basis has an energy cutoff of 400 eV.

### III. RESULTS AND DISCUSSIONS

It is widely recognized that the electronic properties of AGNRs can be categorized into three distinct groups based on their  $E_g$ , which are highly sensitive to the width ( $N$ ) of the ribbon. These categories are typically referred to as  $N = 3p$ ,  $N = 3p + 1$ , and  $N = 3p + 2$ , where  $p$  is an integer. According to the topological classification by Zak phase, for the cases of AGNRs with  $N = 3p$  and  $N = 3p + 1$ , where  $N$  satisfies an odd number, the  $Z_2$  invariant of the system can be expressed as follows [12]:

$$Z_2 = \frac{1 + (-1)^{\lfloor \frac{N}{3} \rfloor + \lfloor \frac{N+1}{2} \rfloor}}{2}, \quad (5)$$

where the floor function  $\lfloor x \rfloor$  takes the largest integer less than or equal to a real number  $x$ . For the cases of  $N = 3p + 2$ , AGNRs is predicted to be semimetal. In the following, for simplicity, we will focus discussion on the case of  $N = 3p$  in detail and the discussion for  $N = 3p + 2$  and  $N = 3p + 1$  in Supplemental Material [52].

In the case of AGNR with  $N = 3p$ , such as  $N = 69$ , we initially observe an  $E_g$  of 0.139 eV without any strain [Fig. 2(a)]. Using Eqs. (4) and (5), we calculate the  $Z_2$  invariant to be 1, indicating that the system is in a topological nontrivial phase in the absence of the strain. The parity eigenvalues of the VBM and the CBM at the  $\Gamma$  point are represented by the red and green dots, respectively, with values of  $-1$  and  $+1$  [Fig. 2(a)]. Interestingly, the  $E_g$  can be effectively controlled by the application of the strain [Figs. 2(b)–2(d)]. As the strain increases, the  $E_g$  decreases [Fig. 2(b)], while the parity eigenvalues of the VBM and CBM remain unchanged. At a critical strain value of  $c_c = 0.01005$ , the  $E_g$  closes, resulting in the formation of a gapless Dirac cone [Fig. 2(c)]. In this

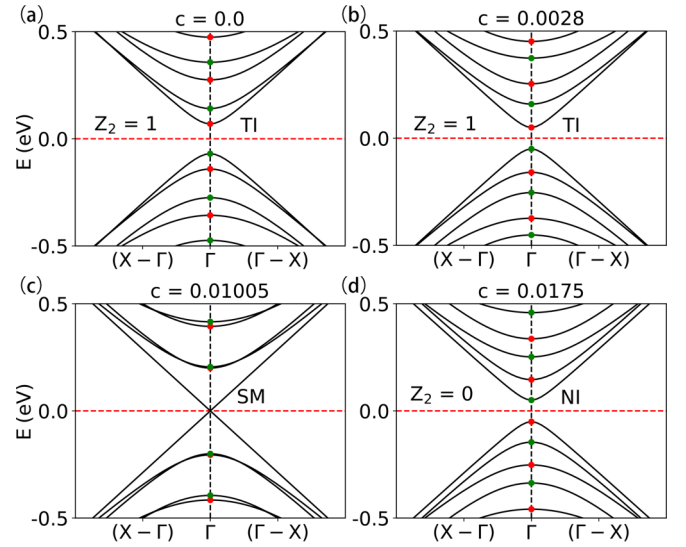


FIG. 2. Band structure of AGNR ( $N = 69$ ) with the different strain (a) for  $c = 0.0$ , (b) for  $c = 0.0028$ , (c) for  $c = 0.01005$ , (d) for  $c = 0.0175$ . The  $Z_2$  invariants are shown in the figures. The labels for SM, TI, and NI represent semimetal, topological insulator, and normal insulator, respectively. The parity eigenvalues  $\langle \psi_{n\Gamma_i} | \hat{M} | \psi_{n\Gamma_i} \rangle$  of the bands near Fermi level at  $\Gamma$  are marked with red dot (green dot) for a value of  $+1$  ( $-1$ ).

semimetallic phase, the  $Z_2$  invariant is not well defined. Upon further increasing the strain, for example, by increasing  $c$  to 0.0175 [Fig. 2(d)], the  $E_g$  reopens, and the parity eigenvalues of the VBM and CBM switch, leading to a calculated  $Z_2$  invariant of 0. This indicates that the system undergoes transition from a topological insulator (TI) phase to a normal insulator (NI) phase, driven by the applied strain. Examining the conduction bands, represented by the red (green) dots, we observe that with increasing the strain, bands with  $+1$  ( $-1$ ) parity eigenvalues at the  $\Gamma$  point move closer (farther) to the Fermi energy. This trend is reversed for the valence bands. This suggests that near the Fermi energy, further increasing the strain will result in repeated interleaving of the topological order of the energy bands. Our subsequent calculations provide further evidence for this phenomenon.

Figure 3 shows the  $E_g$  as a function of the strain, allowing for a broader perspective on how strain affects the topological properties of the system. In the range from  $c = 0$  to  $c = 0.1$ , due to the bands with  $+1$  ( $-1$ ), parity eigenvalues at the  $\Gamma$  point move closer (farther) to the Fermi energy for the conduction bands, multiple topological phase transitions can occur for  $N = 69$ ,  $N = 71$  and  $N = 73$  which belongs to  $N = 3p$ ,  $N = 3p + 2$  and  $N = 3p + 1$ , respectively. For the different cases, the relation for  $E_g$  and the strain is different especially for the first phase transition shown in Figs. 3(a)–3(c). For the case with  $N = 3p$ , as the strain increases, the  $E_g$  decreases and then increases for the first phase transition shown in Fig. 3(a). However, for the  $N = 3p + 2$  and  $N = 3p + 1$ , the  $E_g$  increases, then decreases and then increases for the first phase transition shown in Figs. 3(b)–3(c). However, it is crucial to determine the initial topological state of the AGNRs based on Eq. (5) before analyzing the subsequent topological transitions. This equation serves as a criterion for identifying



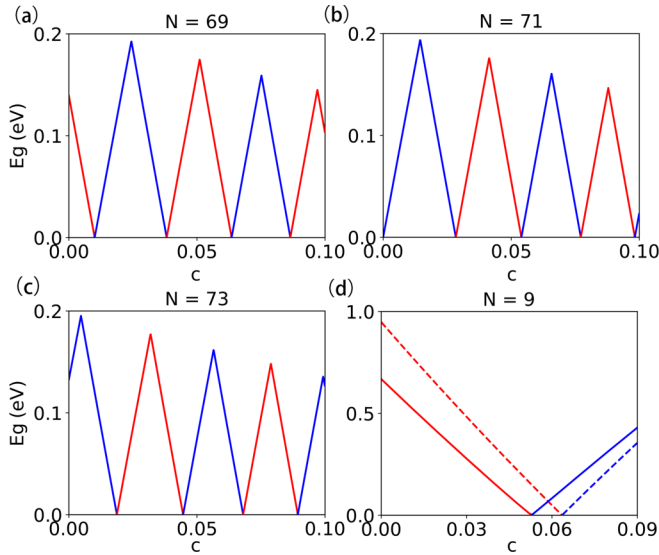


FIG. 3. The band gap versus strain (a) for  $N = 69$ , (b) for  $N = 71$ , (c) for  $N = 73$ , (d) for  $N = 9$ . The  $Z_2$  invariants are shown in the figures. In (a) to (d), the regions with red and blue colors represent the regions with  $Z_2 = 1$  and  $Z_2 = 0$ , respectively. The solid lines in (d) represent the results calculated using DFT, while the dotted lines represent the results obtained from the TB model.

the initial topological phase of the AGNRs. It is worth noting that the specific form of the strain does not significantly impact the results. The conclusions drawn from the analysis remain consistent across all four strain forms considered. Additional calculations involving inhomogeneous strains, such as quadratic power  $u_y = cy^2$  and  $u_y = \begin{cases} cy^2, & y > 0 \\ -cy^2, & y \leq 0 \end{cases}$  and cubic power  $u_y = cy^3$ , yield similar results (refer to the Supplemental Material [52] for more details).

To validate the reliability of the results obtained from the TB model, the influence of strain on the electronic structure of AGNRs is further validated using DFT calculations. In this case, a relatively narrow AGNR with  $N = 9$  (belonging to the  $N = 3p$  category) is chosen. The DFT calculation results are consistent with the TB model, and both curves exhibit the same trend, as shown in Fig. 3(d). Although the transition point (TP) values slightly differ between the TB model ( $c = 0.0635$ ) and DFT ( $c = 0.053$ ), this discrepancy may arise from the choice of TB parameters. From the above discussion, based on both DFT and TB model results, it is confirmed that strain can drive topological phase transitions in AGNRs, and the specific phase transition depends sensitively on the width of the AGNRs.

As discussed earlier, it is known that nanoribbons with different widths exhibit distinct topological properties. A fascinating quantum structure is the heterojunction composed of a finite number of nanoribbons with varying widths. Such heterojunctions give rise to end states (ES) and junction state (JS) due to the diverse topological nature of the electronic structure of the constituent nanoribbons. The ability to manipulate and control these ES and JS may have potential applications in quantum devices. However, achieving precise control over the topological phase and JS in one-dimensional systems remains a challenging task. In the final part of this study, we aim to

investigate the influence of the strain on the ES and JS in heterojunctions composed of flexible AGNR segments with different widths. Based on the calculated  $Z_2$  invariants for various widths, we construct an AGNR heterojunction composed of a 9AGNR ( $N = 9$ ) and a 7AGNR ( $N = 7$ ) which possesses a commensurate zigzag' end termination [12]. The heterojunction, denoted as 9AGNR/7AGNR, is illustrated in Figs. 4(a) and 4(b), with each segment comprising 25 unit cells. We choose the 9AGNR/7AGNR heterojunction as a representative example to investigate the JS and ES, as the existence of these states in the unstrained 9AGNR/7AGNR system has been experimentally confirmed [16].

The  $Z_2$  invariant is 1 and 0 for 9AGNR and 7AGNR without the strain, respectively, as labeled in Fig. 4(a). With the strain depicted in Eq. (1) for  $c = 0.09$ , based on Eq. (4), we find both the 9AGNR and 7AGNR segments have  $Z_2 = 0$ , as labeled in Fig. 4(b). Figure 4(c) shows the density of state (DOS) of the system with (blue dashed line) and without (red solid line) the strain. In Fig. 4(c), we use a Gaussian function  $f(E) = e^{-(E-E_0)^2/\Gamma^2}$  with a broadening factor  $\Gamma = 0.01$  eV to smooth the discontinuous energy spectra.

We observed sharp and equally heightened peaks at  $E_F = 0$  eV in the DOS spectrum, regardless of the presence of the strain. Without the strain, our results are consistent with previous findings. However, previous studies did not show such significant peaks or in-gap states in the DOS for two topologically equivalent segments [12,14]. In contrast, with strain applied, both segments are nontrivial insulating phase in our case, but we still observe equally heightened peaks at  $E_F = 0$  eV. To further illustrate the in-gap states with and without the strain, we plot the charge-density distribution for  $E_F = 0$  eV, as indicated by the black arrow in Fig. 4(c), highlighting the colored carbon atoms. We make the following observations: (i) In the absence of the strain, the in-gap states consist of both JS and ES, which aligns with previous findings. (ii) Under the strain, the in-gap states only comprise ES, a novel observation not reported previously. In other words, regardless of the strain, ES persist at the edge of the 9AGNR, while JS is exclusively present at the interface without the strain. Consequently, the strain can eliminate JS in flexible AGNR heterojunctions.

The underlying physics behind this phenomenon is relatively straightforward. When the strain is applied to the system, the AGNRs of heterojunction change from topologically inequivalent to topologically equivalent, inducing the elimination of JS [12]. To further clarify this point, we calculate the local density of states (LDOS) using a Gaussian function for the left cell, interface, and right cell regions, as denoted by the red and blue dashed rectangles in Figs. 4(a) and 4(b). Regardless of the strain, we observe a sharp peak at  $E_F = 0$  eV in the LDOS of the left cell, as shown in Fig. 4(d). Interestingly, the peak for the heterojunction with the strain (blue dashed line) is larger than that without the strain (red solid line), indicating that the strain significantly enhances the ES of the 9AGNR. Simultaneously, as depicted in Fig. 4(e), a sharp peak at  $E_F = 0$  eV is exclusively present in the interface of the heterojunction without the strain due to the presence of JS. This suggests that strain enhances ES while simultaneously eliminating JS. Furthermore, the LDOS of the right cell does not exhibit a peak at  $E_F = 0$  eV, regardless

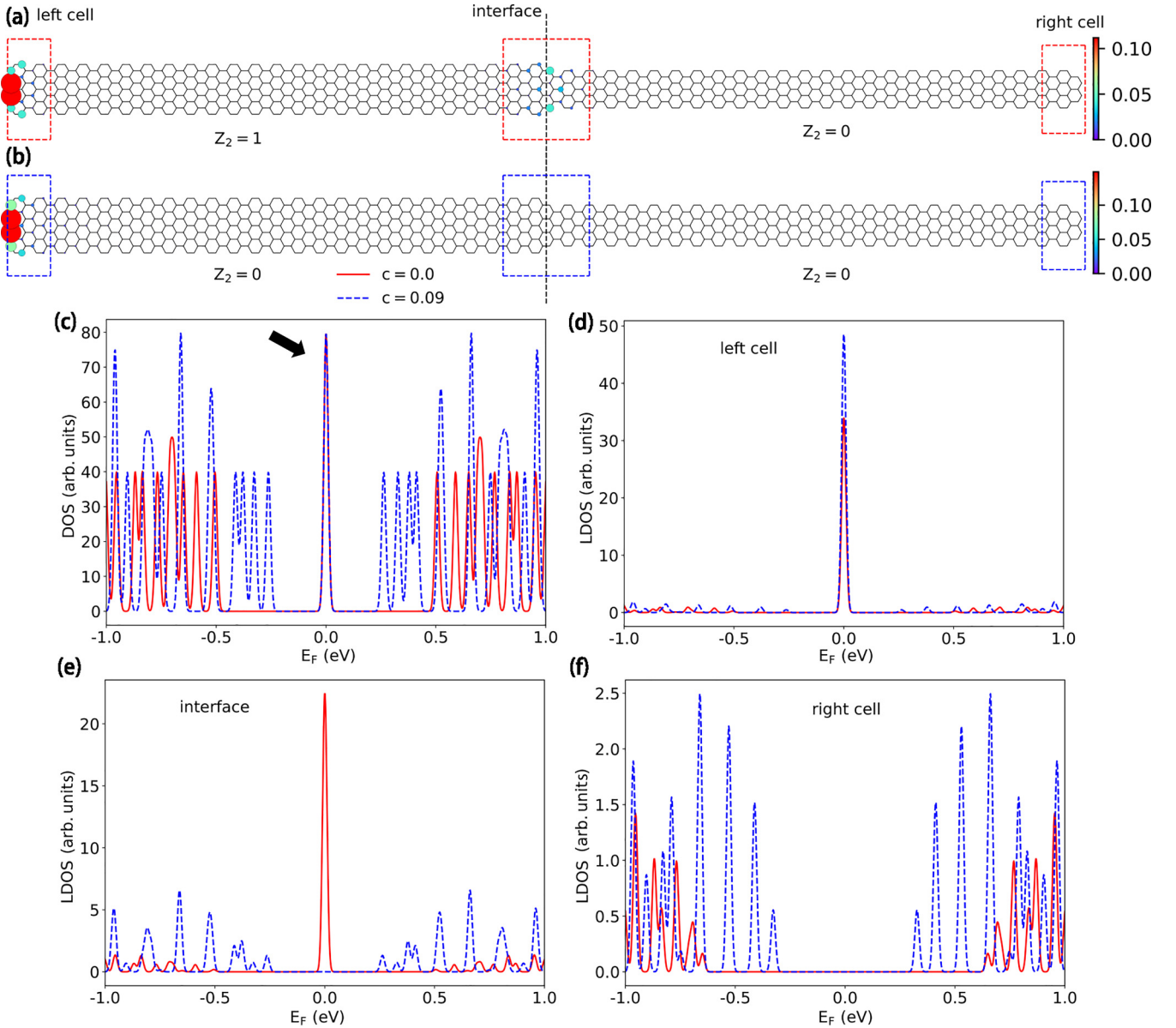


FIG. 4. The heterojunction formed by finite AGNR segments with  $N = 9$  and  $N = 7$  AGNR (9AGNR/7AGNR) containing 25 unit cells. The unstrained and strained heterojunction configurations are depicted in (a) and (b), respectively. The interface between the two nanoribbons is denoted by the black dotted line. The charge-density distribution is represented by the carbon atoms in different colors and sizes, indicating the strength of the charge distribution. The charge density is scaled relative to the state labeled by the black arrow in (c). (c) The DOS of the heterojunction with and without strain. (d)–(f) The LDOS of the heterojunction with and without strain. The red solid and blue dashed lines in (c)–(f) denote the heterojunction with and without strain, respectively. The LDOS in (d)–(f) is obtained by integration in region labeled by the red and blue rectangles in (a) and (b). The  $Z_2$  invariants for two segments are labeled in (a) and (b).

of the strain, indicating the absence of ES in the 7AGNR. This observation can be attributed to the quantum confinement effect, where the narrow width of the 7AGNR prevents the formation of ES (see Fig. 5). And for the AGNR with  $Z_2 = 1$ , the end states have robustness against local perturbations [12]. To align our examination's structure more closely with real experimental material samples, here we consider disorder effects arising from defects or adsorption in the sample material. We introduce disorders by incorporating Anderson disorders. In this context, we perform disorder calculations by adding a randomly, spatially dependent onsite potential with a distribution ranging from  $[-\omega/2, \omega/2]$ , where  $\omega$  is

the intensity of the disorders. Figures 4(a) and 4(b) show the charge distribution without disorders. Introducing disorders, as depicted in Figs. S4(c) and S4(d) in Supplemental Material [52], illustrates that within a certain disorder range, our conclusions remain unaffected under the same strain. For example, with  $\omega = 1.1$  eV, the charge distribution remains essentially the same, regardless of the presence of disorders [Figs. 4(a) and S4(c) or Figs. 4(b) and S4(d)]. Furthermore, the presence or absence of disorders does not hinder the strain's ability to eliminate the junction state. Therefore, we assert that disorders arising in real materials will not impact our results.

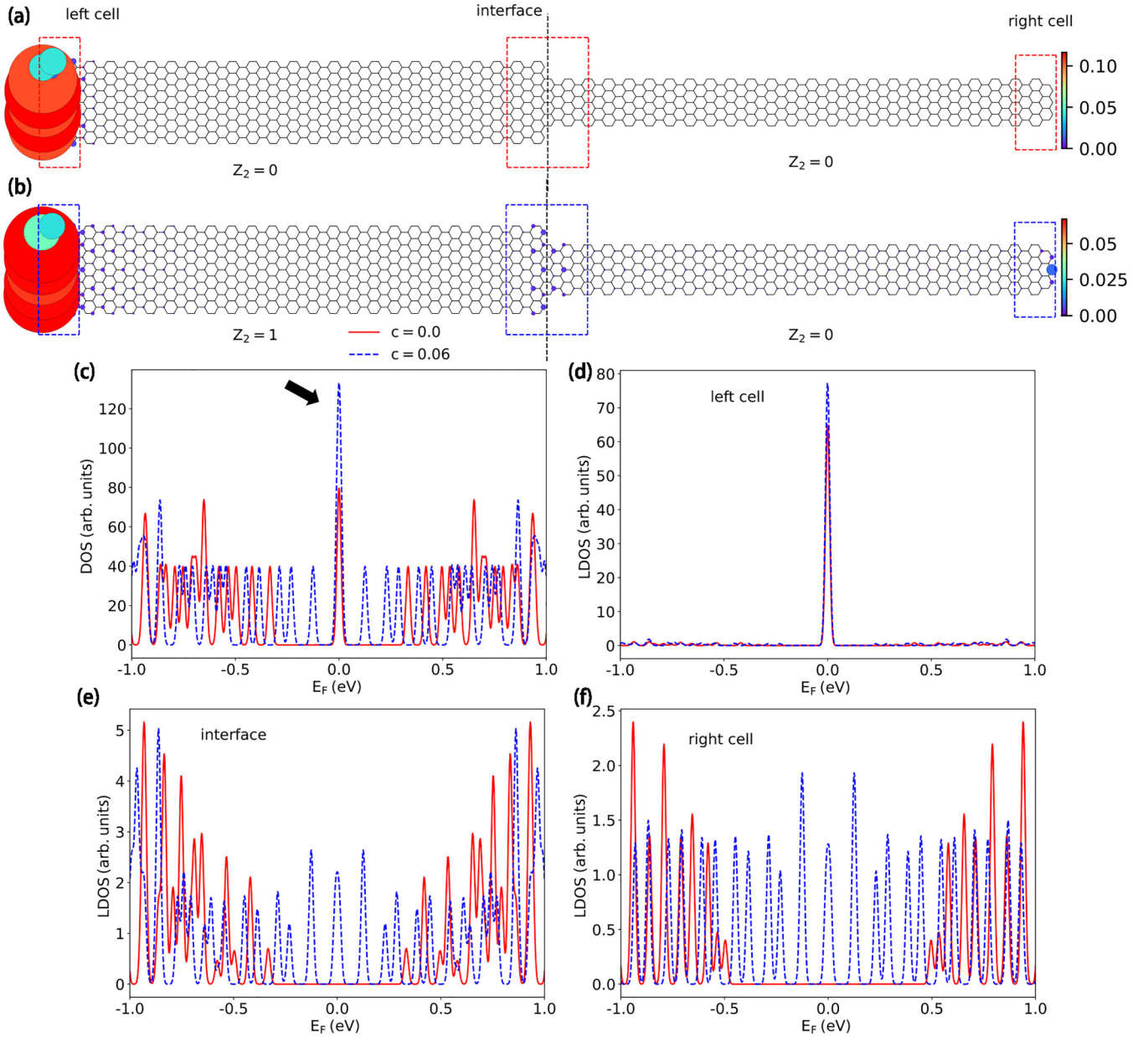


FIG. 5. The heterojunction formed by finite AGNR segments with  $N = 15$  and  $N = 9$  AGNR (15AGNR/9AGNR) containing 25 unit cells. The unstrained and strained heterojunction configurations are depicted in (a) and (b), respectively. The interface between the two nanoribbons is denoted by the black dotted line. The charge-density distribution is represented by the carbon atoms in different colors and sizes, indicating the strength of the charge distribution. The charge density is scaled relative to the state labeled by the black arrow in (c). (c) The DOS of the heterojunction with and without strain. (d)–(f) The LDOS of the heterojunction with and without strain. The red solid and blue dashed lines in (c)–(f) denote the heterojunction with and without strain, respectively. The LDOS in (d)–(f) is obtained by integration in region labeled by the red and blue rectangles in (a) and (b). The  $Z_2$  invariants for two segments are labeled in (a) and (b).

We also investigate the 15AGNR/9AGNR heterojunction, where the  $Z_2$  invariant is 0 for 15AGNR and 9AGNR without the strain, as indicated in Fig. 5(a). However, when a strain with  $c = 0.06$  is applied, the  $Z_2$  invariant changes to 1 for 15AGNR, as shown in Fig. 5(b). Notably, we observe that the strain can enhance the ES and create JS, as depicted in Figs. 5(c)–5(f). Therefore, the strain has the ability to both create or eliminate JS while enhancing ES. This implies that through the application of the strain, we can effectively control and regulate the properties of the ES and JS in the heterojunction.

#### IV. CONCLUSIONS

In summary, we present a novel approach for designing 1D AGNRs with adjustable topological phases by applying the strain. Notably, the strain effect is not limited to a specific strain form. This transition is achieved through the switching of parity eigenvalues of the wave functions at the center of the Brillouin Zone, altering the  $Z_2$  invariant of the system from 1 to 0 or 0 to 1 and effectively driving the topological phase transition. And multiple topological phase transitions can occur with larger strain. Additionally, we propose a new



strategy for manipulating the end states and junction state in heterojunctions formed by different topological segments of AGNRs through the application of the strain. By appropriately tuning the strain, we can either create or eliminate the junction state and enhance the end states in the heterojunction. On one hand, experimentally, through bottom-up approaches using precursor molecules, scientists can atomically design edge shapes, widths, and terminations of the graphene ribbon [24]. On the other hand, in real graphene samples, experimentally, uniaxial strain has been achieved by bending graphene on a flexible substrate [61,62]. Based on these experimental findings, we believe that, with the in-depth research on graphene nanoribbon and the advancement of nano-fabrication technology, we expect that our theoretical proposal might be

experimentally realized. Our study offers a promising avenue for tuning topological phase transitions in flexible quasi-1D materials, controlling and customizing the properties of the junction state and end states.

#### ACKNOWLEDGMENTS

This work was supported by the National Natural Science Foundation of China (NSFC) (Grants No. 11974340 and No. 92265203), the Strategic Priority Research Program of the Chinese Academy of Sciences (Grants No. XDB0460000, No. XDB28000000, and No. XDPB22), the Chinese Academy of Sciences (Grant No. QYZDJ-SSW- SYS001), and the National Key Research and Development Program of China (Grant No. 2018YFA0306101).

- 
- [1] K. v. Klitzing, G. Dorda, and M. Pepper, New method for high-accuracy determination of the fine-structure constant based on quantized hall resistance, *Phys. Rev. Lett.* **45**, 494 (1980).
- [2] D. J. Thouless, M. Kohmoto, M. P. Nightingale, and M. den Nijs, Quantized hall conductance in a two-dimensional periodic potential, *Phys. Rev. Lett.* **49**, 405 (1982).
- [3] C. L. Kane and E. J. Mele, Quantum spin hall effect in graphene, *Phys. Rev. Lett.* **95**, 226801 (2005).
- [4] B. A. Bernevig and S.-C. Zhang, Quantum spin hall effect, *Phys. Rev. Lett.* **96**, 106802 (2006).
- [5] M. König, S. Wiedmann, C. Brüne, A. Roth, H. Buhmann, L. W. Molenkamp, X.-L. Qi, and S.-C. Zhang, Quantum spin hall insulator state in hgte quantum wells, *Science* **318**, 766 (2007).
- [6] L. Fu, C. L. Kane, and E. J. Mele, Topological insulators in three dimensions, *Phys. Rev. Lett.* **98**, 106803 (2007).
- [7] L. Fu and C. L. Kane, Topological insulators with inversion symmetry, *Phys. Rev. B* **76**, 045302 (2007).
- [8] M. Z. Hasan and C. L. Kane, Colloquium: Topological insulators, *Rev. Mod. Phys.* **82**, 3045 (2010).
- [9] X. Qian, J. Liu, L. Fu, and J. Li, Quantum spin Hall effect in two-dimensional transition metal dichalcogenides, *Science* **346**, 1344 (2014).
- [10] B. A. Bernevig, T. L. Hughes, and S.-C. Zhang, Quantum spin hall effect and topological phase transition in HgTe quantum wells, *Science* **314**, 1757 (2006).
- [11] H. Zhang, C.-X. Liu, X.-L. Qi, X. Dai, Z. Fang, and S.-C. Zhang, Topological insulators in Bi<sub>2</sub>Se<sub>3</sub>, Bi<sub>2</sub>Te<sub>3</sub> and Sb<sub>2</sub>Te<sub>3</sub> with a single Dirac cone on the surface, *Nat. Phys.* **5**, 438 (2009).
- [12] T. Cao, F. Zhao, and S. G. Louie, Topological phases in graphene nanoribbons: Junction states, spin centers, and quantum spin chains, *Phys. Rev. Lett.* **119**, 076401 (2017).
- [13] O. Gröning, S. Wang, X. Yao, C. A. Pignedoli, G. Borin Barin, C. Daniels, A. Cupo, V. Meunier, X. Feng, A. Narita, K. Müllen, P. Ruffieux, and R. Fasel, Engineering of robust topological quantum phases in graphene nanoribbons, *Nature (London)* **560**, 209 (2018).
- [14] Y.-L. Lee, F. Zhao, T. Cao, J. Ihm, and S. G. Louie, Topological phases in cove-edged and chevron graphene nanoribbons: Geometric structures,  $Z_2$  invariants, and junction states, *Nano Lett.* **18**, 7247 (2018).
- [15] K.-S. Lin and M.-Y. Chou, Topological properties of gapped graphene nanoribbons with spatial symmetries, *Nano Lett.* **18**, 7254 (2018).
- [16] D. J. Rizzo, G. Veber, T. Cao, C. Bronner, T. Chen, F. Zhao, H. Rodriguez, S. G. Louie, M. F. Crommie, and F. R. Fischer, Topological band engineering of graphene nanoribbons, *Nature (London)* **560**, 204 (2018).
- [17] J.-P. Joost, A.-P. Jauho, and M. Bonitz, Correlated topological states in graphene nanoribbon heterostructures, *Nano Lett.* **19**, 9045 (2019).
- [18] J. Jiang and S. G. Louie, Topology classification using chiral symmetry and spin correlations in graphene nanoribbons, *Nano Lett.* **21**, 197 (2021).
- [19] D.-X. Liu, X.-F. Li, X.-H. Zhang, X. Cao, X.-J. Zhu, and D. Shi, Interface magnetism in topological armchair/cove-edged graphene nanoribbons, *J. Phys. Chem. C* **124**, 15448 (2020).
- [20] Q. Sun, Y. Yan, X. Yao, K. Müllen, A. Narita, R. Fasel, and P. Ruffieux, Evolution of the topological energy band in graphene nanoribbons, *J. Phys. Chem. Lett.* **12**, 8679 (2021).
- [21] F. Zhao, T. Cao, and S. G. Louie, Topological phases in graphene nanoribbons tuned by electric fields, *Phys. Rev. Lett.* **127**, 166401 (2021).
- [22] F. M. Arnold, T.-J. Liu, A. Kuc, and T. Heine, Structure-imposed electronic topology in cove-edged graphene nanoribbons, *Phys. Rev. Lett.* **129**, 216401 (2022).
- [23] L. Jiao, X. Wang, G. Diankov, H. Wang, and H. Dai, Facile synthesis of high-quality graphene nanoribbons, *Nat. Nanotechnol.* **5**, 321 (2010).
- [24] J. Cai, P. Ruffieux, R. Jaafar, M. Bieri, T. Braun, S. Blankenburg, M. Muoth, A. P. Seitsonen, M. Saleh, X. Feng, K. Müllen, and R. Fasel, Atomically precise bottom-up fabrication of graphene nanoribbons, *Nature (London)* **466**, 470 (2010).
- [25] C. Tao, L. Jiao, O. V. Yazyev, Y.-C. Chen, J. Feng, X. Zhang, R. B. Capaz, J. M. Tour, A. Zettl, S. G. Louie, H. Dai, and M. F. Crommie, Spatially resolving edge states of chiral graphene nanoribbons, *Nat. Phys.* **7**, 616 (2011).
- [26] P. Ruffieux, S. Wang, B. Yang, C. Sánchez-Sánchez, J. Liu, T. Dienel, L. Talirz, P. Shinde, C. A. Pignedoli, D. Passerone, T. Dumlaff, X. Feng, K. Müllen, and R. Fasel, On-surface synthesis of graphene nanoribbons with zigzag edge topology, *Nature (London)* **531**, 489 (2016).

- [27] K.-Y. Yoon and G. Dong, Liquid-phase bottom-up synthesis of graphene nanoribbons, *Mater. Chem. Front.* **4**, 29 (2020).
- [28] F. Sols, F. Guinea, and A. H. Castro Neto, Coulomb blockade in graphene nanoribbons, *Phys. Rev. Lett.* **99**, 166803 (2007).
- [29] Z. Z. Zhang, K. Chang, and K. S. Chan, Resonant tunneling through double-banded graphene nanoribbons, *Appl. Phys. Lett.* **93**, 062106 (2008).
- [30] F. Zhai and K. Chang, Theory of huge tunneling magnetoresistance in graphene, *Phys. Rev. B* **77**, 113409 (2008).
- [31] Z. Z. Zhang, Z. H. Wu, K. Chang, and F. M. Peeters, Resonant tunneling through S- and U-shaped graphene nanoribbons, *Nanotechnology* **20**, 415203 (2009).
- [32] H. Wang, H. S. Wang, C. Ma, L. Chen, C. Jiang, C. Chen, X. Xie, A.-P. Li, and X. Wang, Graphene nanoribbons for quantum electronics, *Nat. Rev. Phys.* **3**, 791 (2021).
- [33] J. Li, S. Sanz, N. Merino-Díez, M. Vilas-Varela, A. Garcia-Lekue, M. Corso, D. G. de Oteyza, T. Frederiksen, D. Peña, and J. I. Pascual, Topological phase transition in chiral graphene nanoribbons: from edge bands to end states, *Nat. Commun.* **12**, 5538 (2021).
- [34] J. Li and K. Chang, Electric field driven quantum phase transition between band insulator and topological insulator, *Appl. Phys. Lett.* **95**, 222110 (2009).
- [35] B. Monserrat and D. Vanderbilt, Temperature effects in the band structure of topological insulators, *Phys. Rev. Lett.* **117**, 226801 (2016).
- [36] G. Antonius and S. G. Louie, Temperature-induced topological phase transitions: Promoted versus suppressed nontrivial topology, *Phys. Rev. Lett.* **117**, 246401 (2016).
- [37] J. Liu and D. Vanderbilt, Topological phase transitions in  $(\text{Bi}_{1-x}\text{In}_x)_2\text{Se}_3$  and  $(\text{Bi}_{1-x}\text{Sb}_x)_2\text{Se}_3$ , *Phys. Rev. B* **88**, 224202 (2013).
- [38] B. Wunsch, F. Guinea, and F. Sols, Dirac-point engineering and topological phase transitions in honeycomb optical lattices, *New J. Phys.* **10**, 103027 (2008).
- [39] M. S. Miao, Q. Yan, C. G. Van de Walle, W. K. Lou, L. L. Li, and K. Chang, Polarization-driven topological insulator transition in a GaN/InN/GaN quantum well, *Phys. Rev. Lett.* **109**, 186803 (2012).
- [40] D. Zhang, W. Lou, M. Miao, S.-C. Zhang, and K. Chang, Interface-induced topological insulator transition in GaAs/Ge/GaAs quantum wells, *Phys. Rev. Lett.* **111**, 156402 (2013).
- [41] Y. Li, X. Jiang, Z. Liu, and Z. Liu, Strain effects in graphene and graphene nanoribbons: The underlying mechanism, *Nano Res.* **3**, 545 (2010).
- [42] S. M. Loh, Y.-H. Huang, K.-M. Lin, W. S. Su, B. R. Wu, and T. C. Leung, Quantum confinement effect in armchair graphene nanoribbons: Effect of strain on band gap modulation studied using first-principles calculations, *Phys. Rev. B* **90**, 035450 (2014).
- [43] C. Lee, X. Wei, J. W. Kysar, and J. Hone, Measurement of the Elastic Properties and Intrinsic Strength of Monolayer Graphene, *Science* **321**, 385 (2008).
- [44] K. S. Kim, Y. Zhao, H. Jang, S. Y. Lee, J. M. Kim, K. S. Kim, J.-H. Ahn, P. Kim, J.-Y. Choi, and B. H. Hong, Large-scale pattern growth of graphene films for stretchable transparent electrodes, *Nature (London)* **457**, 706 (2009).
- [45] F. Zhai, X. Zhao, K. Chang, and H. Q. Xu, Magnetic barrier on strained graphene: A possible valley filter, *Phys. Rev. B* **82**, 115442 (2010).
- [46] M. Bellec, U. Kuhl, G. Montambaux, and F. Mortessagne, Manipulation of edge states in microwave artificial graphene, *New J. Phys.* **16**, 113023 (2014).
- [47] Z. Wu, F. Zhai, F. M. Peeters, H. Q. Xu, and K. Chang, Valley-dependent Brewster angles and Goos-Hänchen effect in strained graphene, *Phys. Rev. Lett.* **106**, 176802 (2011).
- [48] Y.-M. Li, X. Zhou, Y.-Y. Zhang, D. Zhang, and K. Chang, Dirac fermions and pseudomagnetic fields in two-dimensional electron gases with triangular antidot lattices, *Phys. Rev. B* **96**, 035406 (2017).
- [49] S. Ke, Y.-M. Li, W.-K. Lou, and K. Chang, Pure magnon valley currents in a patterned ferromagnetic thin film, *Phys. Rev. B* **107**, 104426 (2023).
- [50] E. Cadelano, P. L. Palla, S. Giordano, and L. Colombo, Nonlinear elasticity of monolayer graphene, *Phys. Rev. Lett.* **102**, 235502 (2009).
- [51] X. Wei, B. Fragneau, C. A. Marianetti, and J. W. Kysar, Nonlinear elastic behavior of graphene: Ab initio calculations to continuum description, *Phys. Rev. B* **80**, 205407 (2009).
- [52] See Supplemental Material at <http://link.aps.org/supplemental/10.1103/PhysRevB.109.045408> for the results of the nanoribbon with  $N = 3p + 1$  and  $N = 3p + 2$  and the results and conclusions of the other three strain forms.
- [53] M. Oliva-Leyva and G. G. Naumis, Understanding electron behavior in strained graphene as a reciprocal space distortion, *Phys. Rev. B* **88**, 085430 (2013).
- [54] D. Moldovan, M. Anđelković, and F. Peeters, pybinding v0.9.5: a Python package for tight-binding calculations (2020), <https://doi.org/10.5281/zenodo.4010216>.
- [55] S. Coh and D. Vanderbilt, Pythtb 1.7.2 (2016), <http://www.physics.rutgers.edu/pythtb/>.
- [56] J. Zak, Berry's phase for energy bands in solids, *Phys. Rev. Lett.* **62**, 2747 (1989).
- [57] J.-W. Rhim, J. Behrends, and J. H. Bardarson, Bulk-boundary correspondence from the intercellular Zak phase, *Phys. Rev. B* **95**, 035421 (2017).
- [58] G. Kresse and J. Hafner, Ab initio molecular-dynamics simulation of the liquid-metal–amorphous–semiconductor transition in germanium, *Phys. Rev. B* **49**, 14251 (1994).
- [59] G. Kresse and J. Furthmüller, Efficient iterative schemes for ab initio total-energy calculations using a plane-wave basis set, *Phys. Rev. B* **54**, 11169 (1996).
- [60] J. P. Perdew, K. Burke, and M. Ernzerhof, Generalized gradient approximation made simple, *Phys. Rev. Lett.* **77**, 3865 (1996).
- [61] R. Roldán, A. Castellanos-Gomez, E. Cappelluti, and F. Guinea, Strain engineering in semiconducting two-dimensional crystals, *J. Phys.: Condens. Matter* **27**, 313201 (2015).
- [62] I. Gablech, J. Brodský, P. Vyroubal, J. Piastek, M. Bartošík, and J. Pekárek, Mechanical strain and electric-field modulation of graphene transistors integrated on MEMS cantilevers, *J. Mater. Sci.* **57**, 1923 (2022).